Journal of Rehabilitation in Civil Engineering 11-3 (2023) 68-87

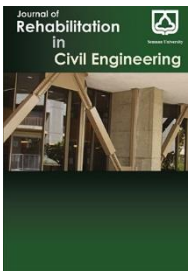

Journal homepage: http://civiljournal.semnan.ac.ir/

Prediction of the Punching Load Strength of SCS Slabs with Stud-Bolt Shear Connectors Using Numerical Modeling and GEP Algorithm

Mehdi Yousefi[1], Mohammad Golmohammadi[2*], Seyed-Hashem Khatibi[3], Majid Yaghoobi[2]

1. Civil Engineering Department, Faculty of Maritime Engineering, Chabahar Maritime University, Chabahar, Iran
2. Civil Engineering and Architectural Department, Faculty of Engineering, University of Torbat Heydarieh, Torbat Heydarieh, Iran
3. Civil Engineering Department, Sistan and Baluchestan University, Zahedan, Iran

Corresponding author: mailto:m.golmohammadi@torbath.ac.ir

ARTICLE INFO

Article history:
Received: 14 March 2022
Revised: 06 August 2022
Accepted: 21 September 2022

Keywords:
Steel-concrete-steel Slab;
Stud-bolt connector;
Finite element;
Gene expression programming;
Failure modes.

ABSTRACT

Using bolt shear connectors in Steel-Concrete-Steel (SCS) slabs is very important due to producing a complete steel plates connection and adjusting the sandwich thickness desirably. Therefore, in the present research, a numerical study is conducted on the flexural behavior of SCS sandwich slabs with stud-bolt shear connectors under the effect of the quasi-static concentrated load. For this purpose, first, the experimental specimens extracted from the previously published study were numerically modeled and quasi-statically analyzed using explicit dynamic analysis. Then based on the tests, the models were validated. Subsequently, the effect of the parameters, including the thickness of steel plates, stud-bolts diameter, the concrete core thickness, center-to-center distance of stud-bolt connectors, and the concrete core strength was evaluated based on the numerical models on the failure modes and the force-displacement curve. Finally, using the experimental setup and gene expression programming (GEP) algorithm, several numerical models were planned to predict the maximum strength of the slabs and a simple relation was proposed. The maximum strength resulting from the proposed relation and numerical models had an acceptable agreement with an error of 11% based on mean absolute percentage error (MAPE).

How to cite this article:
Yousefi, M., Golmohammadi, M., Khatibi, S. H., & Yaghoobi, M. (2023). Prediction of the Punching Load Strength of SCS Slabs with Stud-Bolt Shear Connectors Using Numerical Modeling and GEP Algorithm. Journal of Rehabilitation in Civil Engineering, 11(3), 68-87.
https://doi.org/10.22075/JRCE.2022.26528.1628

1. Introduction

By changing the geometrical combination of common building materials, i.e, steel and concrete, new structures such as steel columns filled with concrete, concrete-filled steel tubular (CFST) form as column under axial compression [1,2], and steel-concrete-steel (SCS) sandwich structures as beam, slab or wall are created. Steel-concrete-steel (SCS) sandwich structures are composed of two steel layers and one concrete core. Solomon et al. [3] proposed this system to be used for making bridges deck. The first use of SCSs began with gluing steel surfaces to a concrete core. However, the adhesive had a weak shear and so, the mechanical connectors were replaced. Some shear connectors mainly noted by researchers are offered in Fig. 1. Double skin composite (DSC) with stud shear connectors as shown in Fig. 1(a) [4], bar shear connectors in Bi-steel system according to Fig. 1(b) [5–7], corrugated-strip shear connectors (CSC) (see Fig. 1(c)) [8,9], middle hook in J-hook shear connectors as– Fig. 1(d) [10,11], separately corrugated strip shear connectors (SCSCs) according to Fig. 1(e)[12–14], and Stud-bolt connectors in SCS according to Fig. 1(f) [15–18].

In the rest of the section, the recent studies on the SCSs are briefly reviewed.

Yousefi and Khatibi [19] conducted an experimental and numerical study on the bending behavior of SCS beams with a new design of shear connectors known as separately corrugated strip shear connectors (SCSCs). In this study, to provide a two-end welded connection of SCSCs at the end of the bases, plug welding was used to create a partial link. The results showed that as a two-end welded connection to steel plates is provided for SCSCs, even partially, the bending strength increases about 30%. Also, finally, equations were offered to predict the bending strength of this system.

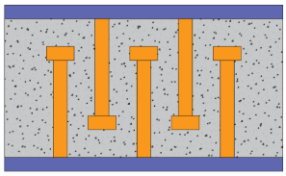

a) Double skin concrete system with stud shear connectors.

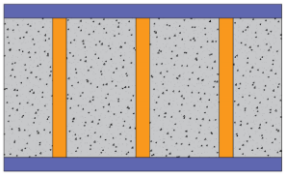

b) bar shear connectors in Bi-steel system.

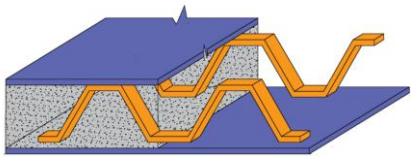

c) corrugated-strip shear connectors (CSC).

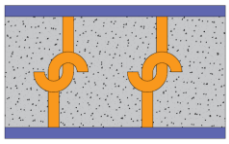

d) J-hook shear connectors.

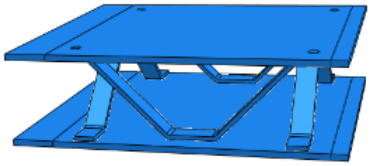

e) separately corrugated strip shear connectors (SCSC).

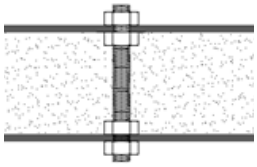

F) Stud-bolt connectors in SCS

Fig 1. Shear connectors in SCS sandwiches.

Chang-Hui Li et al.[20] studied the enhanced Channel's shear connectors in SCS sandwich structures numerically. In this research, after verification of the numerical models based on test data, models were developed to evaluate the effect of the parameters, including diameter and grade of bolts and nuts, connectors distance, and concrete core strength on the shear strength behavior of this system more deeply. Finally, principles were offered to design the enhanced Channel's shear connectors.

Golmohammadi and Ghalehnovi [20] studied the interlayer shear behavior of SCS beams with stud-bolt shear connectors with a high strength under the push-out test. The results showed that the increase in the thickness of steel plates significantly affects the specimen's maximum strength. Also as the concrete thickness increases, the specimen's ultimate full shear strength approaches the bolt's ultimate strength and in addition, ductility increases. On the other hand, it was observed that the increase in the shear connector's diameter directly affects the increase in the specimen's maximum strength and slightly affects the increase in energy absorption.

In the present research, the bending behavior of SCS sandwich slabs is studied numerically with bolt shear connectors with a high strength under the effect of the quasi-static concentrated load. For this purpose, four slab specimens were modeled from the experiments by Golmohammadi and Ghalehnovi [21] first, and then, they were validated. Based on valid models, 11 numerical models were prepared with different parameters. Based on the numerical models, the effect of the parameters, including the thickness of steel faceplates (tp), stud-bolts diameter (D), concrete thickness (hc), concrete strength (fc), and center-to-center distance of stud-bolts (S) is studied on SCS slabs. In the next step of this research, based on the output data of numerical models, the final strength of the SCS slabs with stud-bolts is predicted. Generally, there are various methods to optimize or behavior prediction derived from nature, including genetic programming (GP) [22], artificial neural network (ANN) [23,24], fuzzy logic (FL) [25], adaptive neural-fuzzy inference system (ANFIS) [26,27], probabilistic methods [28] and data-driven models [29–36], group method of data handling (GMDH) [32,33], wavelet analysis [34], etc.

However, the Gene Expression Algorithm (GEP) method, which is based on the GP, has a relatively high accuracy and has been considered by researchers in recent years. Therefore, finally, using the GEP algorithm, an equation is offered to predict the maximum strength of SCS slabs.

2. Finite Element Model

One of the numerical analysis methods that has acceptable accuracy despite its high speed is the explicit dynamic analysis method. Therefore, in the present study, this method was used for the quasi-static analysis of SCS slabs [35] . For this purpose, four specimens of the experiments by Golmohammadi et al. [21], were modeled with the geometrical dimensions in Table 1.

2.1. Geometric Modeling

For modeling, the setting of the slab test is shown in Fig. 2(a). To model the geometry of the test first components, including steel faceplates, stud-bolts buried in the concrete, concrete core and load cell must be created.

A 3D eight-node continuum element (C3D8) is used for modeling. The general mesh sizes 10, 12, and 15 mm were examined and finally, the mesh size 10 mm was chosen due to the more remarkable agreement between the experimental curve and modeling. A more acceptable mesh size is selected to provide a more accurate simulation in the connection regions between the shear connectors and steel plates, and also in the contact regions between the shear connectors and concrete core. In Fig. 2(b), a view of meshing of steel plates, stud-bolts, and concrete core can be observed.

2.2. Materials Modeling

Various models have been presented to predict reinforced concrete behavior. These models can be based on continuum finite element or concrete damage plasticity (CDP) [41,42]. Concrete damage plasticity (CDP) is a suitable method to simulate concrete cracking in Abaqus software [38]. This model is based on the continuous plastic behavior in which two main failure mechanisms are considered, including the compressive crushing and tensile cracking of concrete. CDP model parameters include dilation angle (ψ), eccentricity, biaxial-to-uniaxial compressive strength ratio ($f = f_{b0} / f_{c0}$), stress plane distortion or confinement angle parameter (k) and viscoplastic parameter (μ). The values of these parameters were considered 38°, 0.1, 1.16, 0.667 and 0.001, respectively, based on Abaqus manual [38] and previous numerical researches on SCSs, especially, by Yousefi et al.[13]. Also, the values of the concrete compressive stress-strain diagram were obtained based on the modified Popovics relationship as follows. [39,40]:

$$\sigma_c = \frac{nf_c\varepsilon_c}{\varepsilon_0(n-1+(\frac{\varepsilon_c}{\varepsilon_0})^{nk})} \quad (1$$

$$n = 0.8 + \frac{f_c}{17} \quad (2$$

$$\begin{cases} k = 0.67 + (\frac{f_c}{62}) & \varepsilon_c > \varepsilon_0 \\ k = 1 & \varepsilon_c \le \varepsilon_0 \end{cases} \quad (3$$

Table 1. Specifications of the slabs being tested [21].

Specimen	Dimensions of plate (mm^3)	Concrete thickness (mm)	Stud-bolt diameter (mm)	Stud-bolts' spacing (mm)	Number of holes
SCS B8-3	1200×1200×6	150	8	150	49
SCS B10-2	1200×1200×6	100	10	100	121
SCS B10-3	1200×1200×6	150	10	150	49
SCS B12-2	1200×1200×6	100	12	100	121

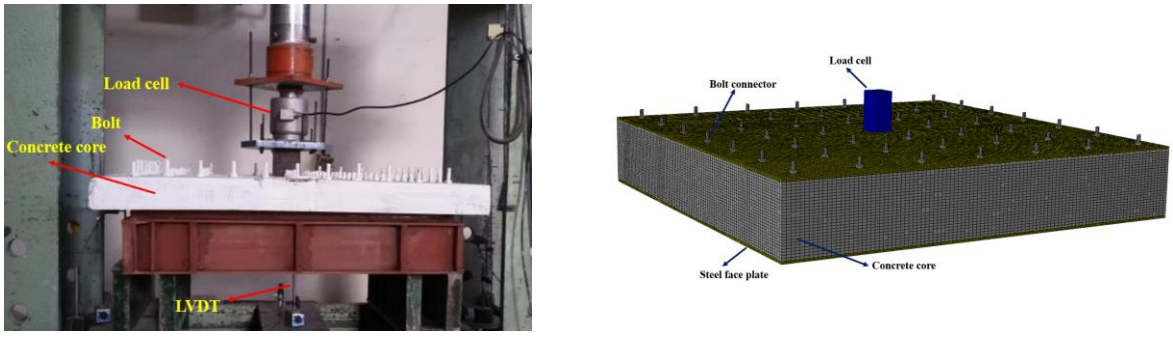

(a) **(b)**

Fig 2. (a) experimental set up of the slab [21] (b) finite elements model of SCS slab.

where, f_c denotes compressive strength of standard cylindrical concrete; ε_0 denotes strain at f_c; σ_c is compressive stress; ε_c is compressive strain. The compressive stress-strain curve of concrete used to model SCS slabs is shown in Fig. 3(a).

On the other hand, the tensile behavior of concrete before cracking is considered linear and after cracking, the fracture energy of cracking (GFI) model is used according to CEB-FIP instructions as follows [41]

$$G_f = G_{f0}\left(\frac{f_c}{10}\right)^{0.7} \quad (4$$

here, G_{f0} is the base fracture energy for ordinary concrete, which depends on maximum aggregate diameter. For normal concrete with aggregates of diameters of 8, 16, and 32 mm, the values of G_{f0} are 0.025, 0.030 and 0.058 (Nmm/mm^2), respectively.

According to Fig. 3(a), with the growth of compression cracks, the stiffness of concrete is reduced. Therefore, the damage index d_c is defined on the softening branch of the stress-strain curve with values between zero and one (zero without damage and one meaning the general decline of strength) to determine the amount of damage. This index is also defined for tensile or cracking concrete as d_t. The values of $d_{c,t}$ in different parts of the softening branch of compressive and tensile diagrams are taken into account in such a way that the stress obtained based on the Eq. (5) matches the stress values of diagrams by trial-and-error. Using Eq. (5) are calculated compressive and tensile stresses ($\sigma_{c,t}$) based on compressive or tensile damage indices ($d_{c,t}$) as follows [42]:

$$\sigma_{c,t} = (1-d_{c,t}).E_0.(\varepsilon_{c,t} - \tilde{\varepsilon}^{pl}_{c,t}) \quad (5$$

where, E_0 is the elastic stiffness of undamaged material and $\tilde{\varepsilon}^{pl}_{c,t}$ can be compressive or tensile plastic strain of concrete. Also, the parameters on Fig. 3, including cracking strain, $\tilde{\varepsilon}^{ck}_t$, and compressive inelastic strain, $\tilde{\varepsilon}^{in}_c$, can be obtained as follows:

$$\tilde{\varepsilon}^{ck}_t = \varepsilon_t - \varepsilon^{el}_{ot} \quad (6$$

$$\tilde{\varepsilon}^{in}_c = \varepsilon_c - \varepsilon^{el}_{oc} \quad (7$$

Here, $\varepsilon^{el}_{ot} = \sigma_t / E_0$ and $\varepsilon^{el}_{oc} = \sigma_c / E_0$ that are tensile and compressive elastic strains for undamaged material, respectively.

The good fit of the curves in the softening branch of Fig. 3(a and b) indicates the correct choice of d_c and d_t values. The values of d_c in the remarked points on the softening branch of the curve in Fig. 3(a) were considered 0.0, 0.1, 0.2, 0.7 and 0.9, respectively. Also, for the concrete tensile damage in Fig. 3(b), the amount of d_t in strains of 0 and 0.00127 is set to 0 and 0.9, respectively. These provide the possibility of numerical modeling of the process of compressive (crushing) and tensile (cracking) damage of concrete [38].

To model steel material, an elastoplastic model is used with Von Mises yield criterion and isotropic strain stiffening rule using the ABAQUS material library. To determine the elastic behavior of steel material, Young's modulus of elasticity E_S and Poisson's ratio ν_s must be defined. For this, at least three repetitions of the test are required for each sheet thickness and each stud-bolt diameter. The plastic behavior of steel plates with thicknesses of 4 and 6 mm, and stud-bolts with diameters of 8, 10 and 12 mm based on Golmohammadi tests are given in Tables 2 and 3 [21].

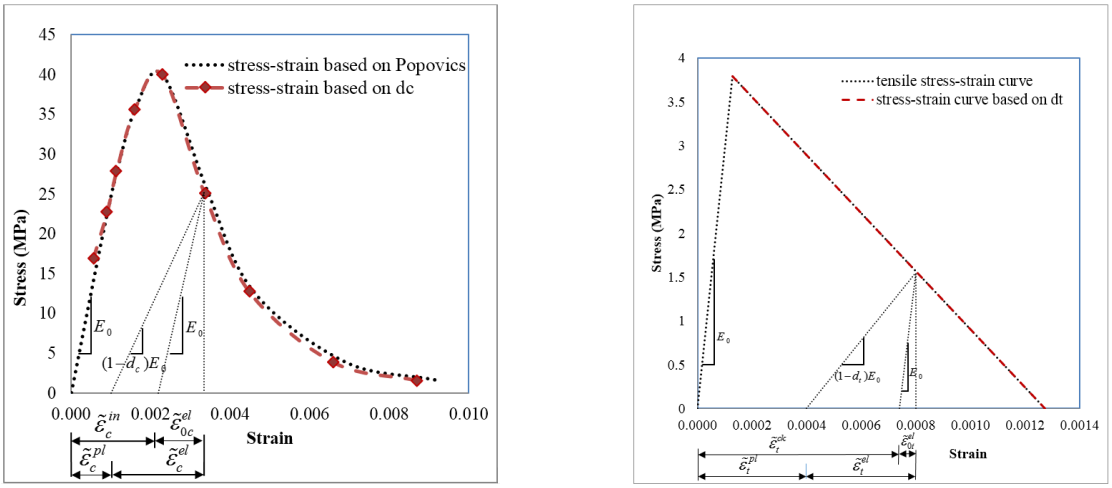

a b

Fig 3. Comparison of the stress-strain curves with the curves obtained from damage indices ($d_{c,t}$) for NWC; a) Compressive curves, b) tensile curves.

Table 2. Required parameters of steel faceplates for FEM simulation.

Thickness (mm)	Yield stress (Mpa)	Maximum stress (Mpa)	Strain in maximum stress	E_s (Gpa)
4	255	385	0.30	206
6	283	490	0.25	204

Table 3. Required parameters of stud-bolt connectors for FEM simulation

Stud-bolt diameter (mm)	Yield stress (Mpa)	Maximum stress (Mpa)	Strain in maximum stress	E_s (Gpa)
8	745	890	0.061	217
10	764	867	0.058	205
12	730	908	0.057	207

2.3. Boundary Conditions and Contacts

In the modeling of SCS slab test according to Fig. 4, SCS slab is placed on supports consisting of 4 rebars that are fixed in all directions (Ux = Uy = Uz = 0). According to Fig. 2(a), the rigid component is loaded quasi-statically. The contact between concrete and steel plates, and that between shear connectors and concrete core are simulated as surface to surface with Hard Contact formulation in the normal direction and frictionless in the tangential direction. Due to the modeling complexity and to save time, mass scaling is used in Explicit Solver for quasi-static analysis.

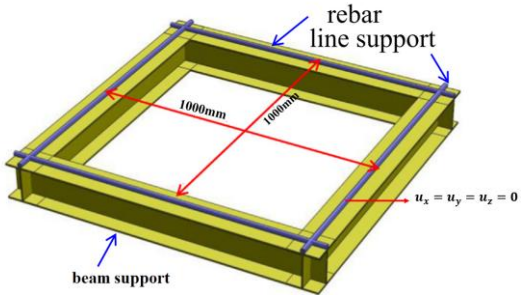

Fig 4. Support for the test.

3. Validation of FE model

To ensure quasi-static loading in all models using mass scale in the explicit dynamic analysis, it was controlled that the kinetic energy would not exceed 10% of internal energy. Then, by comparing the failure modes and load-displacement curves of the models with experimental results, the validity of numerical models was ensured.

3.1. Validation Based on Failure Modes and Force-Displacement Curves

Fig. 5(a-d) shows that FE has been able to simulate a variety of failure modes, including shear and flexural cracks, and buckling of the upper steel faceplate. Fig. 6(a-d) compares the load-displacement curves from the modeling and the experimental. For this purpose, numerical models with three mesh sizes of 10, 12 and 15 mm have been created. According to the figure, using FE, the trend of the curves in terms of the elastic and plastic area has been acceptable. However, there are errors in the curves, one of the reasons for which is the simplification of the properties of steel materials and the assumption of isotropic materials for concrete. Also in Table 4, for validation of numerical models, the maximum strength of the tested samples and the one predicted based on numerical modeling are compared. According to the table, the mean and coefficient of variance (C.O.V.) of the predicted maximum strength to the maximum strength of the experimental are 0.976 and 0.004, respectively. Therefore, it can be concluded that the maximum force obtained from the experiments had an acceptable correlation with the numerical results.

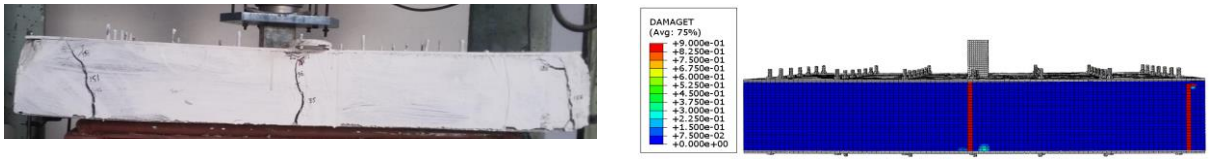

a) SCS B8-3.

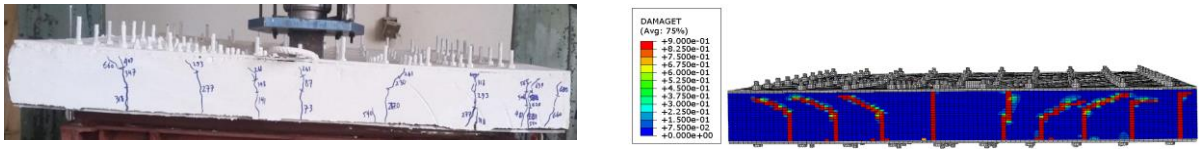

b) SCS B10-2.

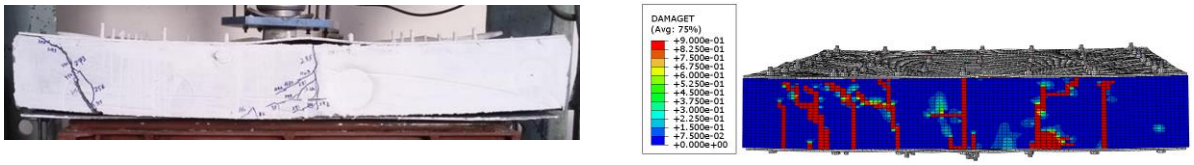

c) SCS B10-3.

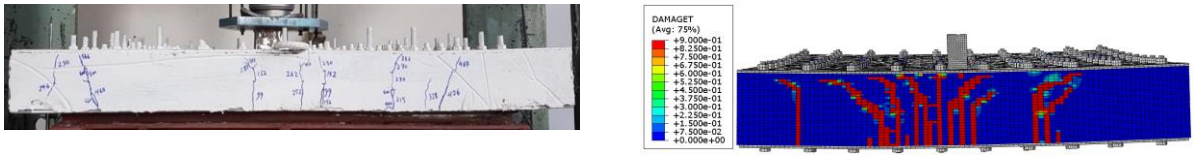

d) SCS B12-2.

Fig 5. Failure modes of experimental and FEA results.

Table 4 . The comparison of the maximum strength obtained from the experiment and FEA.

Specimen	F_{ut} by test (kN)	F_{un} by FEA (kN)	$\frac{F_{un}}{F_{ut}}$
SCS B8-3	398.52	424.39	1.065
SCS B10-2	688.81	614.18	0.892
SCS B10-3	535.56	542.5	1.013
SCS B12-2	637.34	596.82	0.936
Average			**0.976**
C.O.V.			**0.004**

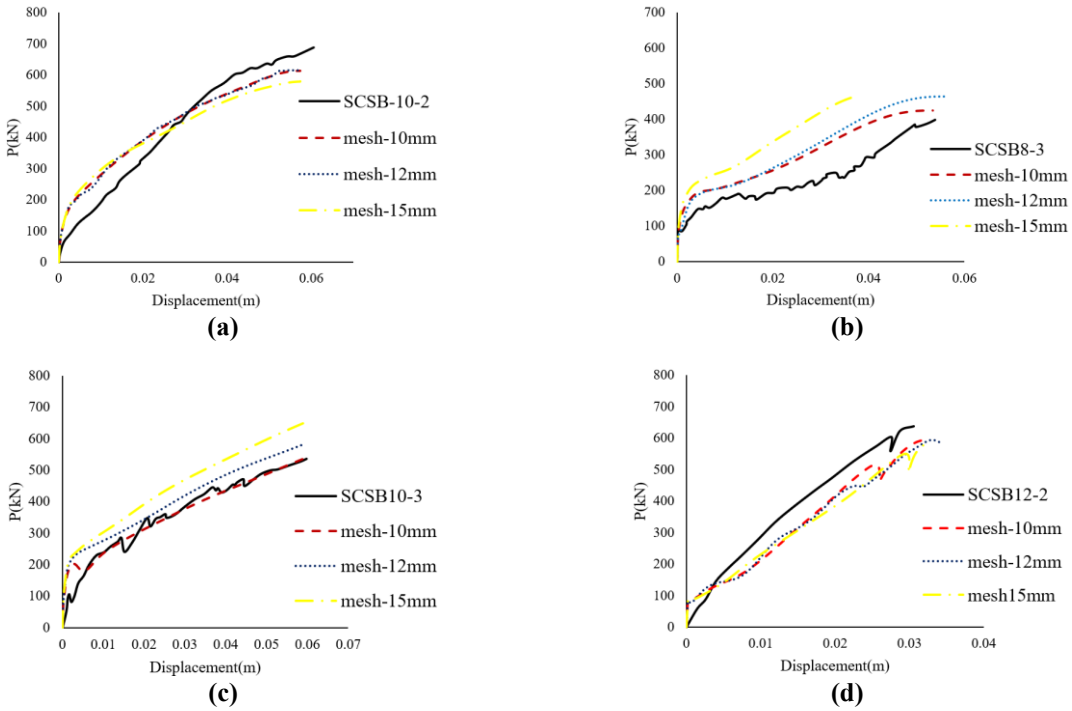

Fig 6. Load–displacement curves of tests and FE analyses.

4. The parameters of the Study

In this research, by modeling 11 numerical specimens according to Table 5, the effects of the concrete thickness, h_c, thickness of steel faceplate, t_p, the diameter of stud-bolt shear connectors, D, center-to-center distance of stud-bolts, S, and the compressive strength of concrete, f_c, are investigated.

Table 5. FE models properties.

Slab	D(mm)	S(mm)	t_p(mm)	h_c(mm)	f_c(MPa)
S1	8	100	4	80	38.5
S2	10	100	4	80	38.5
S3	12	100	4	80	38.5
S4	8	150	4	80	38.5
S5	8	300	4	80	38.5
S6	8	100	6	80	38.5
S7	8	100	10	80	38.5
S8	8	100	4	150	38.5
S9	8	100	4	250	38.5
S10	8	100	4	80	50
S11	8	100	4	80	60

4.1. The Effect of the Diameter (D) Of Stud-Bolt Shear Connectors

Fig. 7 shows the effect of the diameter of stud-bolt shear connectors on the load-displacement curve and failure modes. According to the Fig. 7(a), by increasing the stud-bolts diameter from 8 to 10 and 12 mm, the maximum strength has increased from 715.97 kN to 742.75 kN and 830.69 kN, respectively. In other words, by increasing the diameter of the stud-bolts from 8 to 10 mm, there is no significant improvement in the maximum strength of the slab and only the initial stiffness has increased. However, as the diameter increased from 8 to 12 mm, in addition to the relative increase in the initial stiffness, an increase in the maximum strength (16%) can be observed. Fig. 7(b) shows that as the diameter increases to 12 mm, fewer stud-bolts pass the yield limit. Therefore, the probability of stud-bolt rupture is reduced, greater stiffness and strength are expected, and ultimately the integrity of the composite is maintained.

4.2. The Effect of the Center-To-Center Distance (S) Of Stud-Bolt Shear Connectors

In Fig. 8, the effect of the distance on the shear connectors is observed on the load-displacement curve and failure modes. As shown in Fig. 8 (a), increasing the distance of the connectors has a significant effect on stiffness, maximum strength and energy absorption. So that by increasing the distance from 100 to 150 mm, the maximum strength has decreased by about 14% from 715.97 kN to 613.02 kN, and by increasing the distance to 300 mm, it has decreased by about 40% and reached 428.51 kN.

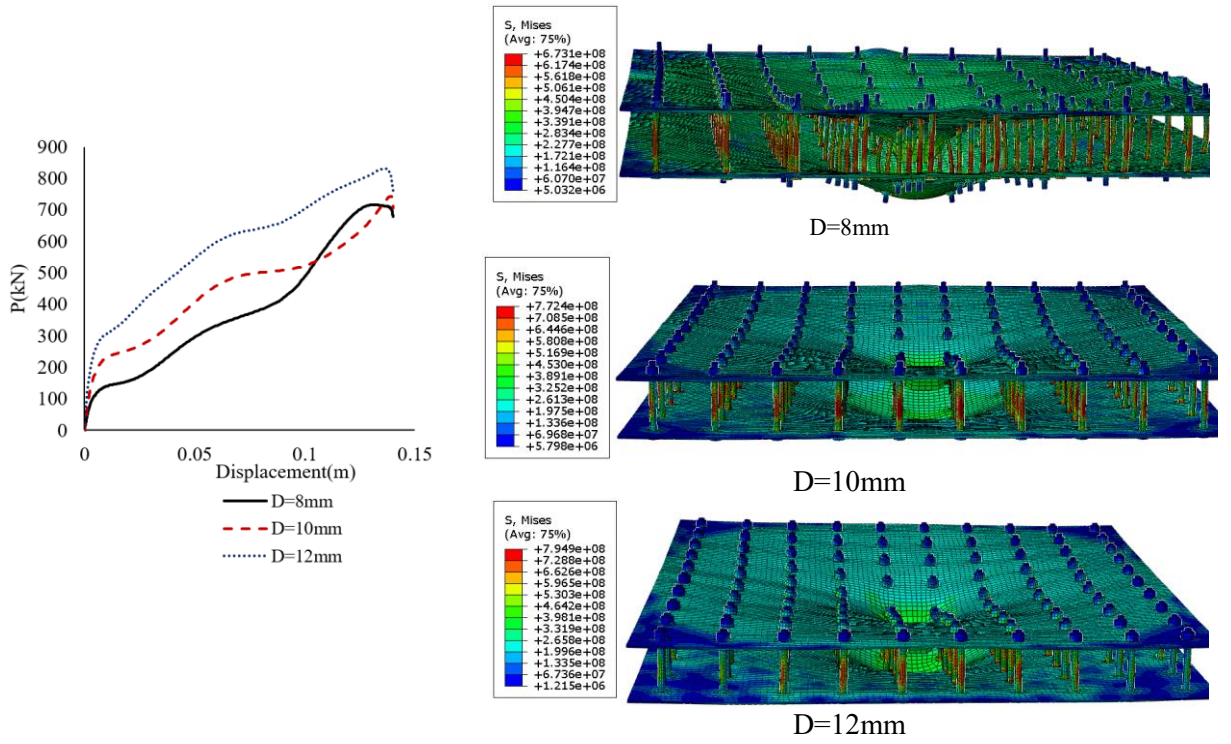

a **b**

Fig 7. The diameter of the stud-bolt shear connectors.

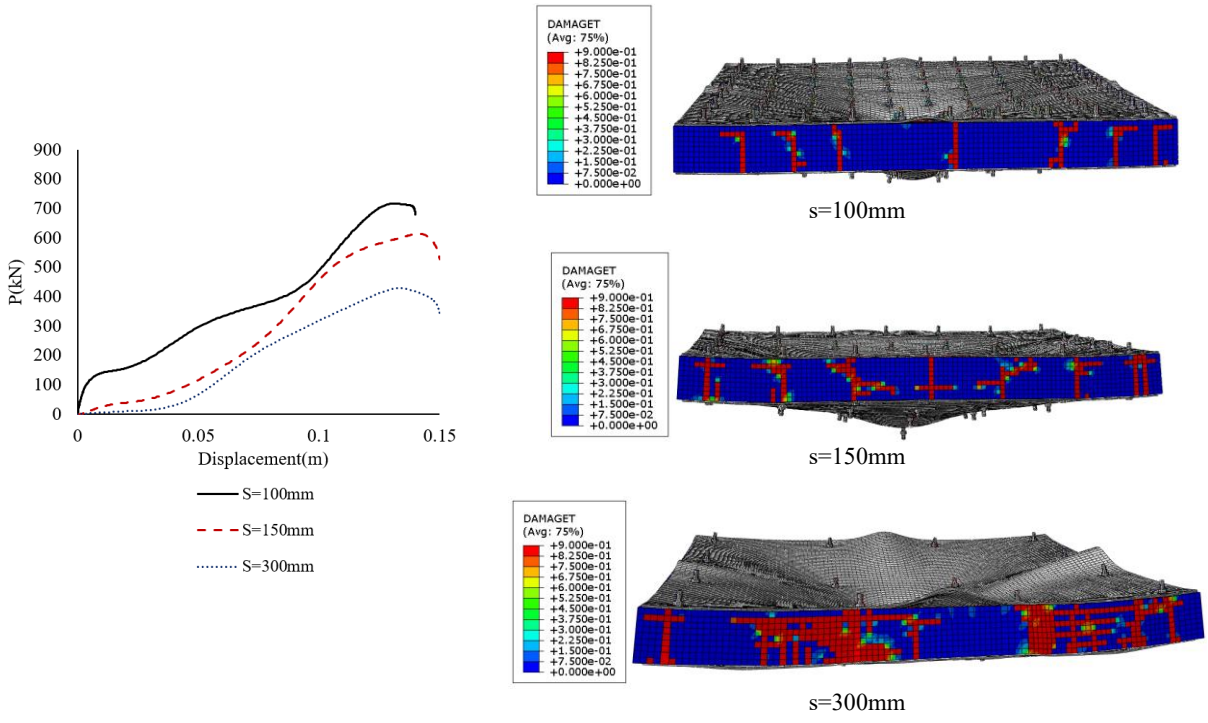

Fig 8. Spacing of the stud-bolt shear connectors.

According to the figure, increasing the distance of the connectors from 100 to 150 and 300 mm has caused the energy absorption of the samples to decrease by about 18% and 43% from 53655 kN.mm, respectively. The curves also show a significant reduction in initial stiffness. Fig. 8(b) shows that increasing the distance between the connectors weakens the connection of the steel faceplates and eventually separates them from the concrete core. Because of this, diagonal cracks will develop and as a result, the composite performance of the slab will be weaker.

4.3. The Effect of Steel Faceplates Thickness (T_p)

Three numerical slab samples are modeled with steel faceplates thickness of 4, 6 and 10 mm. The results of failure modes and load-displacement curves are shown in Figure 9. According to the curves in Fig. 9(a), it can be seen that by increasing the thickness of steel faceplates from 4 to 6 and 10 mm, in addition to increasing the initial stiffness, the maximum strength has increased by about 1.32 and 2.19 times the initial value (31.8% and 119.37%, respectively). The failure modes in Fig. 9(b) show that the ductility decreases with the excessive increase in the thickness of the steel plates. In other words, since bending cracks, shear cracks and crushing of the concrete core can be observed, it seems using thicker than necessary steel plates will cause complete failure in concrete and thus steel plates capacity will go to waste in a less ductile manner.

4.4. The Effect of Concrete Core Thickness (h_c)

Another parameter affecting the flexural behavior of SCS slabs can be the thickness of the concrete core. Hence, three numerical

models with different thicknesses of concrete cores were created. The curves in Fig. 10(a) indicate that as the concrete core thickness increased from 80 mm to 150 mm and 250 mm, the maximum strength increased by about 46% and 88%, respectively. The trend of the diagram indicates that the increase in the concrete thickness results in an increase in stiffness, strength and ductility. However, in the plastic area can be seen a longer path before the start of membrane activity of steel plates and re-ascent of the diagram, which indicates early cracking of the concrete core, especially in thickness of 250 mm. According to Fig. 10(b), the failure modes indicate that with the increase of the core thickness, the bending cracks have turned into diagonal shear cracks. One of the solutions to this problem can be to increase the dimensions of stud-bolts and steel plates against increasing concrete thickness.

4.5. The Effect of Concrete Strength (f_c)

According to Fig. 11, it is concluded that as the concrete strength increased from 38.5 MPa to 50 MPa and 60 MPa, the maximum strength has increased from 715.97 kN to 810.80 kN (by about 13% increase) and 879.88 kN (by about 23% increase), respectively. Therefore, the strength of the concrete core will have a significant effect on the maximum strength of the SCSs.

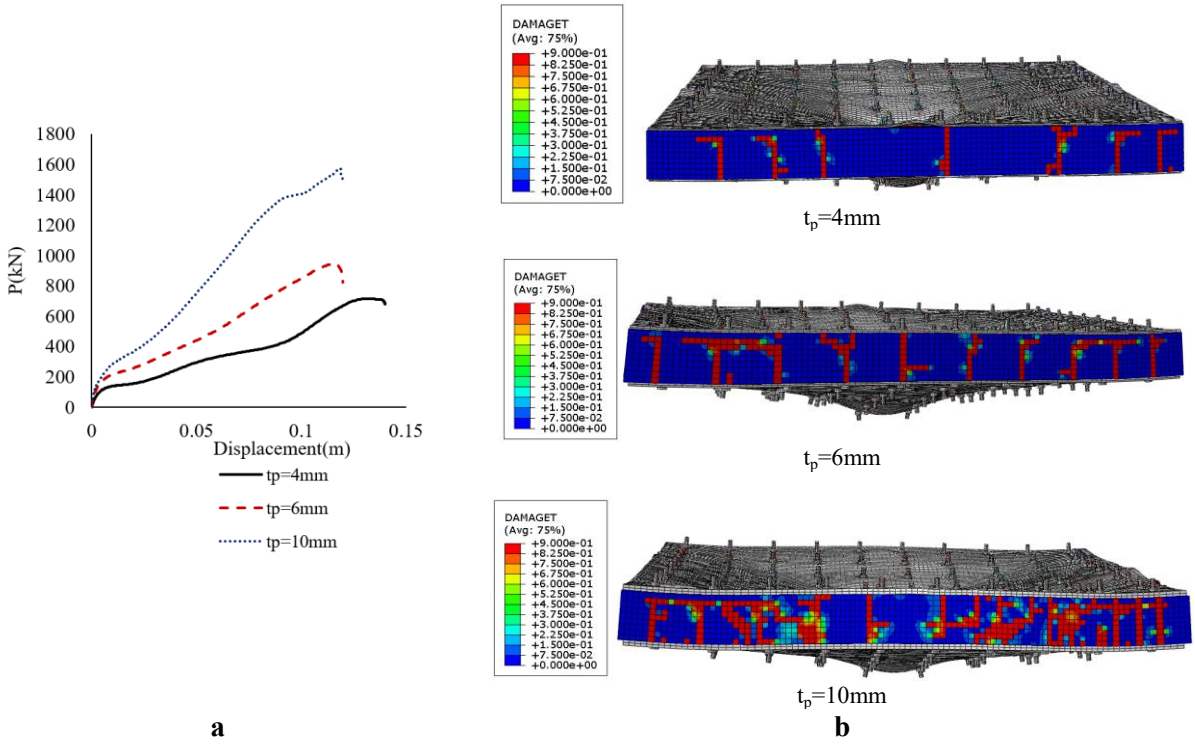

Fig 9 steel faceplates thickness (t_p).

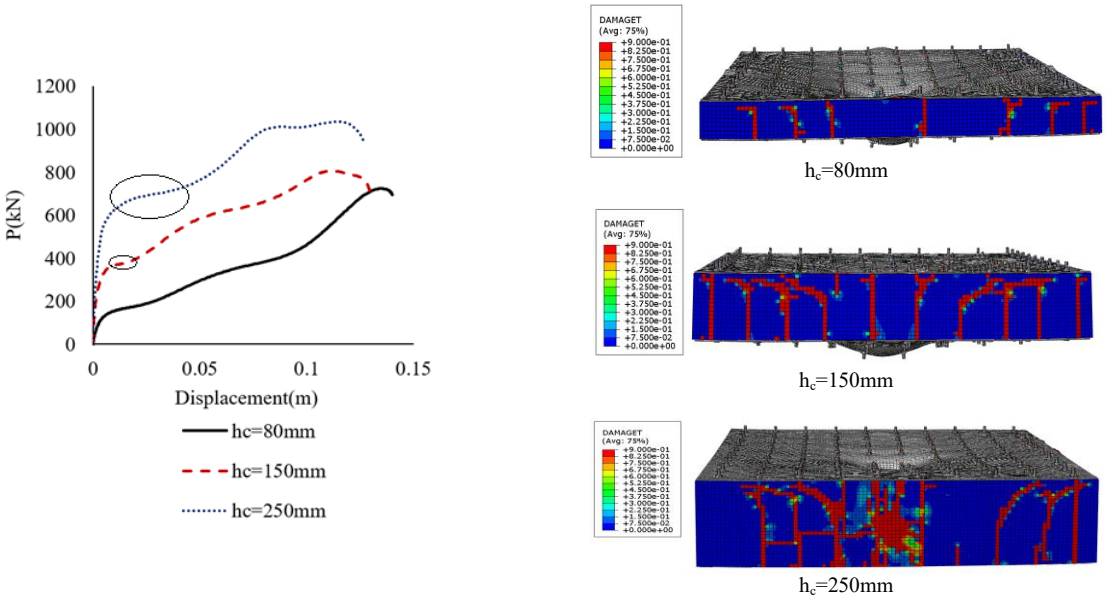

Fig 10. Concrete core thickness (h_c).

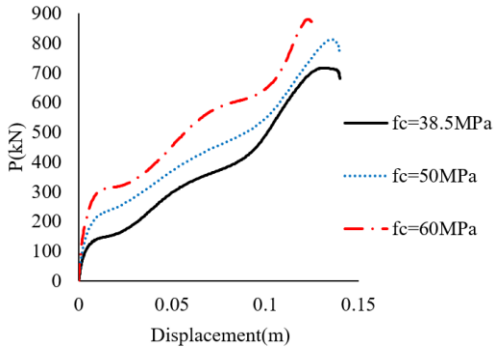

Fi. 11. Concrete strength (f_c).

5. The Proposed Relation of the Prediction of the Maximum Strength of SCS Slabs Using GEP

In 2001, Ferreira proposed a new algorithm called Genetic Expression Programming (GEP) based on Genetic Programming (GP) and Genetic Algorithm (GA). This algorithm is a computer program coded in linear chromosomes with a constant length [48]. GEP creates a symbolic regression using GA genetic operators. The purpose of this program is to produce a mathematical function using the data presented [44]. The GEP algorithm is shown in Fig. 12.

For this purpose, Design of Experiment (DOE) is used to take the effect of the interaction of the geometrical parameters into account [45]. Therefore, five input factors are considered as the input variables as listed in table 6, including stud-bolt diameter (D), the distance of shear connectors (S), steel faceplates thickness (t_p), concrete core thickness (h_c) and concrete core strength (fc).

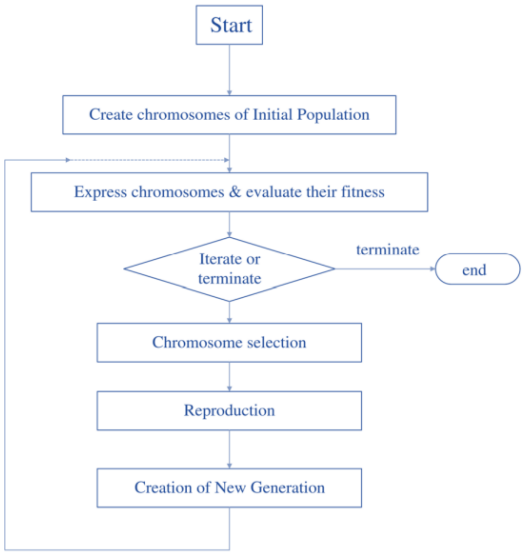

Fig 12. Flow chart of GEP Algorithm[46] .

Then, the specimens were programmed and modeled using the two-level factorial method according to Table 7 in 16 designs with different geometrical parameters. The maximum strength was obtained according to Table 7. To predict the maximum strength of SCS slabs with stud-bolt shear connectors using the GEP, it is assumed that the mechanical properties of steel structures are constant and only the geometrical properties and concrete strength have changed. Considering 16 numerical models in Table 7 and 11 numerical models in Table 5 to examine the failure modes and the effect of geometrical parameters, 27 numerical models became available for the GEP in total. Among 27 numerical models according to Table 8, 20 models were considered for training based on artificial intelligence, and seven models were considered for testing and controlling the results. The programming parameters of the GEP algorithm are given in Table 9. In this program, the competency criterion minimizes the root mean squared error (RMSE).

Table 6. Input parameters and their different levels.

Parameters	Parameters naming	Units	level	
			min	max
stud-bolt diameter	D	mm	8	12
distance of shear connectors	S	mm	100	300
steel faceplates thickness	t_p	mm	4	10
concrete core thickness	h_c	mm	100	150
concrete core strength	f_c	MPa	40	60

Table 7. Details and results of different cases in FE parametric studies.

Slab	D (mm)	S (mm)	t_p (mm)	h_c (mm)	f_c (MPa)	F_{uN} by FEA (kN)
N-1	8	100	4	150	40	1094.20
N-2	8	100	10	150	60	1759.70
N-3	8	100	4	100	60	947.53
N-4	8	100	10	100	40	1570.40
N-5	12	100	10	150	40	1752.28
N-6	12	300	4	150	40	932.71
N-7	12	100	4	150	60	1204.94
N-8	8	300	10	150	40	804.75
N-9	12	300	4	100	60	676.38
N-10	8	300	10	100	60	894.98
N-11	12	100	10	100	60	2070.20
N-12	12	300	10	100	40	1173.50
N-13	8	300	4	150	60	461.02
N-14	12	100	4	100	40	1180.00
N-15	8	300	4	100	40	493.25
N-16	12	300	10	150	60	1568.27

Table 8. The number of training and testing data.

Data type	Number	Percent(%)
Training	20	74
Test	7	26

Table 9. GEP model parameters [24].

Function set	×, /, cube root(3Rt), mul3
Chromosomes	25-35
Head size	8
Number of genes	3
Linking function	Multiplication
Mutation rate	0.045
Inversion rate	0.1
One-point recombination rate	0.3
Two-point recombination rate	0.3
Gene recombination rate	0.1
Gene transposition rate	0.1
Fitness Function Error Type	RMSE

The outputs obtained from the GEP based on 100 different runs led to different equations to estimate the maximum strength of the slab with stud-bolt shear connectors. Finally, the most optimal equation was offered to result from the GEP based on the minimal root mean square error as Eq (8):

$$F_{u(prop)} = 21.34\left(\frac{t_p^2 D^2 h_c f_c}{S}\right)^{\frac{1}{3}} \quad (8$$

Fig. 13 indicates a comparison of the numerical modeling results and the data results predicted by GEP with training and testing data.

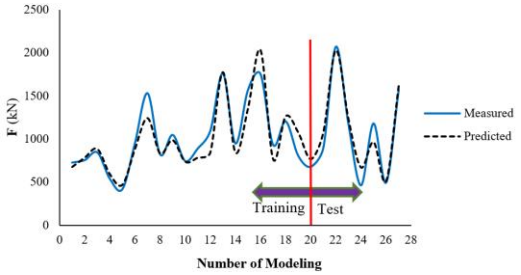

Fig 13. Comparison of the data predicted by Eq.(8) with the modeling data.

For a more accurate assessment, the proposed relationship is evaluated using 4 error measurement parameters, including correlation coefficient (R), Mean Absolute Percentage Error (MAPE), Overall index (OI), and Nash–Sutcliffe Efficiency (NSE), which can be seen in Eqs. 9 to 12, respectively.

$$R = \frac{\sum_{i=1}^{n}(V_{\exp} - \bar{V}_{\exp})(V_{pre} - \bar{V}_{pre})}{\sqrt{\sum_{i=1}^{n}(V_{\exp} - \bar{V}_{\exp})^2}\sqrt{\sum_{i=1}^{n}(V_{pre} - \bar{V}_{pre})^2}} \quad (9$$

$$MAPE = \frac{\sum_{i=1}^{n}\left|\left(\frac{V_{\exp} - V_{pre}}{V_{\exp}}\right)\right|}{n} \times 100 \quad (10$$

$$\begin{cases} OI = \frac{1}{2}\left[2 - \frac{RMSE}{V_{\exp}^{\max} - V_{pre}^{\min}} - \frac{\sum_{i=1}^{n}(V_{\exp} - V_{pre})^2}{\sum_{i=1}^{n}(V_{\exp} - \bar{V}_{\exp})^2}\right] \\ 0 < OI < 1 \end{cases} \quad (11$$

$$\begin{cases} NSE = 1 - \frac{\sum_{i=1}^{n}(V_{\exp} - V_{pre})^2}{\sum_{i=1}^{n}(V_{\exp} - \bar{V}_{\exp})^2} \\ -\infty < NSE < 1 \end{cases} \quad (12$$

In Eqs. 9 to 12, V_{exp} and V_{pre} are the experimental and predicted values; $\bar{V}_{exp}$ and $\bar{V}_{pre}$ are the average of the experimental and predicted values; V_{exp}^{max} and V_{pre}^{min} are the maximum of the experimental values and the minimum of the predicted values, respectively; and n is the total number of samples. Also, the RMSE parameter in Eq. 11 is the Root-Mean-Square Error, which is calculated according to Eq. 13. It should be noted that the best values for MAPE, OI, NSE, and R parameters are 0, 1, 1, and 1, respectively [20].

$$RMSE = \frac{\sqrt{\sum_{i=1}^{n}(V_{\exp} - V_{pre})^2}}{n} \quad (13$$

Further, in Table 10, using error measurement parameters, all Eqs. 9-12 were examined.

Based on the data in the table, it can be concluded that the correlation coefficient (R) of the proposed relation by the authors is 0.939, which indicates a relatively high linear relationship between the variables. Also, the Nash–Sutcliffe Efficiency (NSE) and performance index (OI) values of the proposed relation are 0.879 and 0.929, respectively. Therefore, the ability to estimate the presented relation can be relatively good. In addition, the error rate of the relation was obtained using the Mean Absolute Percentage Error (MAPE) criterion of 11%. According to the results, it can be concluded that the presented relation to estimate the maximum strength of stud-bolt shear connectors has performed relatively well.

Table 10. Comparison of error measurement parameters

Equation	Index			
	R	OI	**MAPE(%)**	**NSE**
Proposed Eq. (8)	0.939	0.929	11	0.879

6. Comparison of Maximum Strength of Slabs Based on Relations and FEA

In Table 11, the maximum strength of 27 numerical models are compared with the values of the proposed relation and previous presented relation by Golmohammadi et al. [21]. Golmohammadi et al. were presented Eq. (14) based on the inter-layer shear strength of stud-bolt connectors (P_R) and the yield line theory of slabs as follows

$$F_p = \frac{n_t (P_R)(h_c + t_p)}{l}\left(\frac{L_s}{L - c} - 0.172\right) \quad (14$$

$$P_R = 0.047 t_p^{0.22} f_c^{0.3} \left(\frac{h_c}{d}\right)^{0.46} A_s \quad (15$$

$$l = L_s / 2\cos(\theta) \quad (16$$

where, n_t is the number of stud-bolts in the square slab, L_s is the dimensions of slab test sample, L is the span length between supports, and c is the length of loading rigid component's side. According to Table 11, the accuracy of the proposed relation is significantly higher than Eq. (14). This problem can be due to the limited number of experiments in the previous study compared to the number of numerical models in the current study, as well as the acceptable accuracy of the GEP method in extracting the appropriate relation.

On the other hand, since the mean and coefficient of variance (C.O.V.) of the ratio of the strength obtained from the proposed relation (Eq. (8)) to the modeling strength are 1.006 and 0.021, respectively, it can be said that the proposed relation has predicted the maximum strength of the numerical models with a perfect approximation. In Fig. 14, the distribution of the FEA results is compared with the values obtained from proposed relation. Also, a domain with an error of less than 15% is considered as a safe domain and the rest as an unsafe domain. It seems that most maximum strength values obtained from Eq. (8) are in the safe domain of the curve.

Table 11. Comparison of bending capacity of slabs based on relations and numerical method.

Slab	F_{uN} by FEA (kN)	$F_{u(Golmohamadi)}$ [21] (kN)	$\frac{F_{u(Golmohamadi)}}{F_{uN}}$	$F_{u(prop)}$ (kN)	$\frac{F_{u(prop)}}{F_{uN}}$
S1	715.97	386.02	0.539	674.24	0.942
S2	754.32	544.31	0.722	782.38	1.037
S3	843.34	720.75	0.855	883.5	1.048
S4	613.02	156.32	0.255	589	0.961
S5	428.51	51.04	0.119	467.49	1.091
S6	951.432	432.08	0.454	883.5	0.929
S7	1570.63	505.96	0.322	1241.95	0.791
S8	806.93	944.99	1.171	831.4	1.03
S9	1035.87	1971.48	1.903	985.74	0.952
S10	810.8	417.50	0.515	735.61	0.907
S11	879.88	440.97	0.501	781.70	0.888
N-1	1094.2	955.89	0.874	842.06	0.77
N-2	1759.7	1372.09	0.78	1775.56	1.009
N-3	947.53	604.99	0.638	842.06	0.889
N-4	1570.4	693.15	0.441	1355.01	0.863
N-5	1752.28	2268.48	1.295	2032.51	1.16
N-6	932.71	236.01	0.253	765.07	0.82
N-7	1204.94	2015.65	1.673	1263.1	1.048
N-8	804.75	160.65	0.20	1075.47	1.336
N-9	676.38	149.37	0.221	765.07	1.131
N-10	894.98	103.51	0.116	1075.47	1.202
N-11	2070.2	1461.61	0.706	2032.51	0.982
N-12	1173.5	171.14	0.146	1231.1	1.049
N-13	461.02	142.75	0.31	668.35	1.45
N-14	1180	1000.23	0.848	963.92	0.817
N-15	493.25	70.48	0.144	510.04	1.034
N-16	1568.27	388.76	0.216	1613.2	1.029
Average			**0.601**		**1.006**
C.O.V.			**0.353**		**0.021**

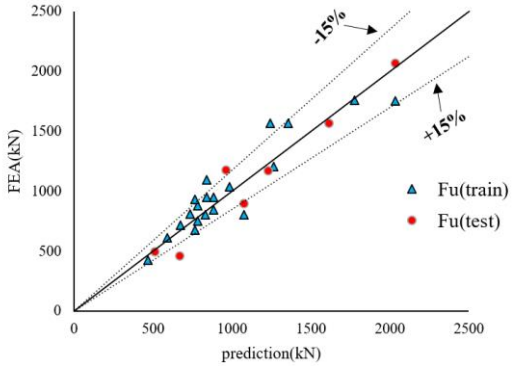

Fig. 14. Comparisons between the numerical analysis results and predictions by proposed Eq.(8).

7. Conclusions

In this study, the first, four test specimens of SCS slab with stud-bolt shear connectors were simulated, and then, the failure modes and load-displacement curves were verified. Afterward, numerical models were made to examine the effect of the geometrical parameters and concrete strength on the maximum strength of the SCS slab, using the GEP algorithm, an equation was proposed to estimate the maximum strength of the slab with stud-bolt shear connectors. After analyzing the numerical specimens, the following results were obtained:

- The maximum strength is directly related to the diameter of stud-bolt shear connectors, as the diameter of the shear connectors increased from 8 to 12 mm, the slab's maximum strength increased about by 16%.

- As the center-to-center distance of the shear connectors increased, shear cracks appeared in the concrete core that could not be treated.

- As the thickness of steel plates increased irregularly, the concrete core ruptured before the steel plates, preventing the composite performance of the concrete.

- As expected, the increase in the concrete core thickness will result in an increase in the stiffness and maximum strength. In addition, the concrete failure will change from flexural failure to shear failure.

- As the concrete strength increases from 38.5 to 60.0 MPa, the slab's maximum strength will increase by about 23%.

- The maximum strength resulting from the proposed relation and numerical models had an acceptable agreement based on several accuracy evaluation methods. For example, the error calculated by MAPE was by about 11%.

Author Contribution statement:

Formal analysis, Seyed Hashem Khatibi (S.H.KH.) and Mehdi Yousefi (M.Y.); Supervision, methodology, M.Y. and Mohammad Golmohammadi (M.G.M.); Investigation, software, M.Y. and S.H.KH; Writing–original draft, S.H.KH and M.Y.; Writing–review & editing, M.Y. and Majid Yaghoobi (MA.Y). All authors have read and agreed to the published version of the manuscript.

Funding: This research received no external funding.

Data Availability: a. Some or all data, models, or code that support the findings of this study are available from the corresponding author upon reasonable request.

Conflicts of Interest: The authors declare no conflict of interest.

Acknowledgments: The authors wish to thank Chabahar Maritime University (CMU),

University of Sistan and Baluchestan (USB) and University of Torbat Heydarieh (UTH).

References

[1] Mahdavi N, Salimi M, Ghalehnovi M. Experimental study of octagonal steel columns filled with plain and fiber concrete under the influence of compressive axial load with eccentricity. J Rehabil Civ Eng 2021;9:01–18. https://doi.org/10.22075/JRCE.2020.17989.1345.

[2] Saberi H, Zadeh VK, Mokhtari A, Saberi V. Investigating of the effect of concrete confinement on the axial performance of circular concrete filled double-skin steel tubular (CFDST) long columns. J Rehabil Civ Eng 2020;8:43–59. https://doi.org/10.22075/JRCE.2020.19167.1362.

[3] Solomon SK, Smith DW, Cusens AR. Flexural tests of steel-concrete-steel sandwiches. Mag Concr Res 1976;28:13–20. https://doi.org/10.1680/macr.1976.28.94.13.

[4] Wang Z, Yan J, Lin Y, Fan F, Yang Y. Mechanical properties of steel-UHPC-steel slabs under concentrated loads considering composite action. Eng Struct 2020;222:111095.

[5] Guo YT, Tao MX, Nie X, Qiu SY, Tang L, Fan JS. Experimental and Theoretical Studies on the Shear Resistance of Steel-Concrete-Steel Composite Structures with Bidirectional Steel Webs. J Struct Eng (United States) 2018;144:1–14. https://doi.org/10.1061/(ASCE)ST.1943-541X.0002182.

[6] Xie M, Foundoukos N, Chapman JC. Static tests on steel-concrete-steel sandwich beams. J Constr Steel Res 2007;63:735–50. https://doi.org/10.1016/j.jcsr.2006.08.001.

[7] Xie M, Chapman JC. Developments in sandwich construction. J Constr Steel Res 2006;62:1123–33. https://doi.org/10.1016/j.jcsr.2006.06.025.

[8] Leekitwattana M, Boyd SW, Shenoi RA. An alternative design of steel-concrete-steel sandwich beam. Science (80-) 2010:1–10.

[9] Leekitwattana M. Analysis of an alternative topology for steel-concrete-steel sandwich beams incorporating inclined shear connectors 2011.

[10] Sohel KMA, Richard Liew JY, Koh CG. Numerical modelling of lightweight Steel-Concrete-Steel sandwich composite beams subjected to impact. Thin-Walled Struct 2015;94:135–46. https://doi.org/10.1016/j.tws.2015.04.001.

[11] Yan JB, Hu H, Wang T. Flexural behaviours of steel-UHPC-steel sandwich beams with J-hook connectors. J Constr Steel Res 2020;169:106014. https://doi.org/10.1016/j.jcsr.2020.106014.

[12] Yousefi M, Ghalehnovi M. Push-out test on the one end welded corrugated-strip connectors in steel-concrete-steel sandwich structure. Steel Compos Struct 2017;24:23–35. https://doi.org/10.12989/scs.2017.24.1.023.

[13] Yousefi M, Ghalehnovi M. Finite element model for interlayer behavior of double skin steel-concrete-steel sandwich structure with corrugated-strip shear connectors. Steel Compos Struct 2018;27:123–33. https://doi.org/10.12989/scs.2018.27.1.123.

[14] Ghalehnovi M, Yousefi M, Karimipour A, de Brito J, Norooziyan M. Investigation of the Behaviour of Steel-Concrete-Steel Sandwich Slabs with Bi-Directional Corrugated-Strip Connectors. Appl Sci 2020;10:8647. https://doi.org/10.3390/app10238647.

[15] Mohammad Golmohammadi, Mansour Ghalehnovi. Investigation on the interlayer shear behavior on steel-concrete-steel sandwich structure with high strength stud bolt connectors. Concr Res Q J 2017;10:45–31. https://doi.org/10.22124/jcr.2017.2556.

[16] Yan C, Wang Y, Zhai X, Meng L. Strength assessment of curved steel-concrete-steel sandwich shells with bolt connectors under concentrated load. Eng Struct 2020;212:110465. https://doi.org/10.1016/j.engstruct.2020.110465.

[17] Golmohammadi M, Ghalehnovi M. Testing and numerical modelling of Steel-Concrete-Steel with stud bolts connectors subject to push-out loading. J Rehabil Civ Eng 2018;0:1–15. https://doi.org/10.22075/jrce.2018.12432.1214.

[18] Karimipour A, Ghalehnovi M, Golmohammadi M, de Brito J. Experimental Investigation on the Shear Behaviour of Stud-Bolt Connectors of Steel-Concrete-Steel Fibre-Reinforced Recycled Aggregates Sandwich Panels. Materials (Basel) 2021;14:5185. https://doi.org/10.3390/ma14185185.

[19] Yousefi M, Hashem Khatibi S. Experimental and numerical study of the flexural behavior of steel–concrete-steel sandwich beams with corrugated-strip shear connectors. Eng Struct 2021;242:112559. https://doi.org/10.1016/j.engstruct.2021.112559.

[20] Li C-H, Yan J-B, Guan H-N. Finite element analysis on enhanced C-channel connectors in SCS sandwich composite structures. Structures 2021;30:818–37. https://doi.org/10.1016/j.istruc.2021.01.050.

[21] Golmohammadi M, Ghalehnovi M, Yousefi M. Experimental Investigation of Steel-concrete-steel Slabs with Stud Bolt Connectors Subjected to Punching Loading. AUT J Civ Eng 2019;3:93–106. https://doi.org/10.22060/AJCE.2018.14763.5496.

[22] Shakeri MS. The Relation between Deposited Weight and Quality of Coating in EPD Method Derived by Genetic programming. Comput Eng Phys Model 2021. https://doi.org/https://doi.org/10.22115/CEPM.2020.239389.1117.

[23] Jahangir H, Rezazadeh Eidgahee D. A new and robust hybrid artificial bee colony algorithm – ANN model for FRP-concrete bond strength evaluation. Compos Struct 2021;257:113160. https://doi.org/10.1016/j.compstruct.2020.113160.

[24] Naderpour H, Mirrashid M. A computational model for Compressive Strength of Mortars Admixed with Mineral Materials,. Comput Eng Phys Model 2018;1:16–25.

[25] Shaffiee Haghshenas S, Shaffiee Haghshenas S, Abduelrhman MA, Zare S, Mikaeil R. Identifying and Ranking of Mechanized Tunneling Project's Risks by Using A Fuzzy Multi-Criteria Decision Making Technique. J Soft Comput Civ Eng 2022;6:29–45. https://doi.org/10.22115/scce.2022.305718.1366.

[26] Khademi A, Behfarnia K, Kalman Šipoš T, Miličević I. The Use of Machine Learning Models in Estimating the Compressive Strength of Recycled Brick Aggregate Concrete. Comput Eng Phys Model 2021;4:1–25. https://doi.org/10.22115/cepm.2021.297016.1181.

[27] Emami H, Emami S. Application of whale optimization algorithm combined with adaptive neuro-fuzzy inference system for estimating suspended sediment load. J Soft Comput Civ Eng 2021;5. https://doi.org/10.22115/SCCE.2021.281972.1300.

[28] Feng D-C, Chen S-Z, Azadi Kakavand MR, Taciroglu E. Probabilistic model based on Bayesian model averaging for predicting the plastic hinge lengths of reinforced concrete columns. J Eng Mech 2021;147:4021066.

[29] Azadi Kakavand MR, Sezen H, Taciroglu E. Data-driven models for predicting the shear strength of rectangular and circular reinforced concrete columns. J Struct Eng 2021;147:4020301.

[30] Rezazadeh Eidgahee D, Jahangir H, Solatifar N, Fakharian P, Rezaeemanesh M. Data-driven estimation models of

asphalt mixtures dynamic modulus using ANN, GP and combinatorial GMDH approaches. Neural Comput Appl 2022;34:17289–314. https://doi.org/10.1007/s00521-022-07382-3.

[31] Azadi Kakavand MR, Allahvirdizadeh R. Enhanced empirical models for predicting the drift capacity of less ductile RC columns with flexural, shear, or axial failure modes. Front Struct Civ Eng 2019;13:1251–70.

[32] Naderpour H, Rezazadeh Eidgahee D, Fakharian P, Rafiean AH, Kalantari SM. A new proposed approach for moment capacity estimation of ferrocement members using Group Method of Data Handling. Eng Sci Technol an Int J 2020;23:382–91. https://doi.org/10.1016/j.jestch.2019.05.013.

[33] Darvishan E. The punching shear capacity estimation of FRP-strengthened RC slabs using artificial neural network and group method of data handling. J Rehabil Civ Eng 2021;9:102–13.

[34] Jahangir H, Khatibinia M, Mokhtari Masinaei M. Damage detection in prestressed concrete slabs using wavelet analysis of vibration responses in the time domain. J Rehabil Civ Eng 2022;10:37–63.

[35] Hibbitt" K&, Inc S. ABAQUS, S.M. and Manual, E.U.s. Pawtucket, RI, USA 2010.

[36] Azadi Kakavand MR, Taciroglu E. An enhanced damage plasticity model for predicting the cyclic behavior of plain concrete under multiaxial loading conditions. Front Struct Civ Eng 2020;14:1531–44.

[37] Azadi Kakavand MR, Neuner M, Schreter M, Hofstetter G. A 3D continuum FE-model for predicting the nonlinear response and failure modes of RC frames in pushover analyses. Bull Earthq Eng 2018;16:4893–917.

[38] Hibbitt K& S. ABAQUS User's Manual. ABAQUS/CAE User's Man 2012:1–847.

[39] Popovics S. A numerical approach to the complete stress-strain curve of concrete. Cem Concr Res 1973;3:583–99. https://doi.org/10.1016/0008-8846(73)90096-3.

[40] Thorenfeldt E. Mechanical properties of high-strength concrete and applications in design. Symp. Proceedings, Util. High-Strength Concr. Norway, 1987, 1987.

[41] Code C-FM. Comité euro-international du béton. Bull d'information 1993;213:214.

[42] Lee J, Fenves GL. Plastic-damage model for cyclic loading of concrete structures. J Eng Mech 1998;124:892–900.

[43] Ferreira C. Gene Expression Programming in Problem Solving. Soft Comput. Ind., London: Springer London; 2002, p. 635–53. https://doi.org/10.1007/978-1-4471-0123-9_54.

[44] Muñoz D. Thesis Discovering unknown equations that describe large data sets using genetic programming techniques. Masters Thesis, Linköping Inst Technol 2005.

[45] Kleppmann W. Statistische Versuchsplanung. Mas. Handb. Qual., vol. 158, München: Carl Hanser Verlag GmbH & Co. KG; 2014, p. 499–522. https://doi.org/10.3139/9783446439924.022.

[46] Fakhrian S, Behbahani H, Mashhadi S. Predicting post-fire behavior of green geopolymer mortar containing recycled concrete aggregate via gep approach. J Soft Comput Civ Eng 2020;4:22–45. https://doi.org/10.22115/SCCE.2020.220919.1182.